http://dx.doi.org/10.5012/bkcs.2012.33.9.3091

X-ray Crystallographic Structure of TIR-Domain from the Human TIR-Domain Containing Adaptor Protein/MyD88-Adaptor-Like Protein (TIRAP/MAL)

Ju Rang Woo, Sunmin Kim,† Steven E. Shoelson, and SangYoun Park†,*

Joslin Diabetes Center & Department of Medicine, Harvard Medical School, Boston, MA 02215
*†School of Systems Biomedical Science, Soongsil University, Seoul, Korea. *E-mail: psy@ssu.ac.kr*
Received May 8, 2012, Accepted May 31, 2012

Key Words : TIR-domain containing Adaptor Protein (TIRAP), MyD88-Adaptor Like protein (MAL), Toll signalling, Toll/Interleukin Receptor (TIR)

Toll-like receptors (TLRs) and interleukin-1 receptors (IL-1Rs) have integral roles in host immune and inflammatory response. In TLR signalling, pathogens bind to the receptor, and stimulate the cytoplasmic Toll/interleukin-1 receptor (TIR)-domain to recruit other TIR-domain containing proteins. Recruitment of one or more of these TIR-domain proteins, such as MyD88, TIRAP/MAL, TRIF/TICAM-1 and TIRP/TRAM/TICAM-2, to the receptors ultimately results in the downstream activation of transcription factors (*e.g.* NF-κB), which induce genes necessary for the host defense.[1,2]

The principal function of the TIR-domain is presumably in the formation of heteromeric assembly of the receptors and adaptors in the signal transduction process. Crystal structures of TIR-domains from TLR1, TLR2, TLR10 and IL-1RAPL, and solution structure of TIR-domain from MyD88 have been reported.[3-6] More recently, crystal structures of plant TIR-domain from *Arabidopsis thaliana* and bacterial TIR-domain from *Paracoccus denitrificans* have been also reported.[7,8] From these studies, several associations mediating the TIR-TIR interaction have been suggested, but the molecular interface involved in the assembly of multiple TIR-domains still remains unclear.

TIRAP (TIR-domain containing Adaptor Protein), also known as MAL (MyD88-Adaptor-Like), functions in pair with MyD88 in the downstream of TLR2 and TLR4 signalling.[9-11] TIRAP is composed of an N-terminal phosphatidylinositol 4,5-bisphosphate (PIP2) - binding domain which is required for membrane localization and a C-terminal TIR-domain which functions primarily to recruit MyD88 to the activated TLR4.[12] TIRAP TIR-domain is conserved among various species (Fig. 1(a)).

In humans, carriage of TIRAP Ser180-to-Leu (S180L) polymorphism conferred protection against infectious diseases possibly by the attenuation of TLR2 signal transduction,[13,14] and Asp96-to-Asn (D96N) showed impaired TLR signaling, which resulted from prevention of MyD88 recruitment to the plasma membrane.[15] The analysis of TIRAP structure would further allow us to propose the consequences of these variants in regard to TIR-domain interactions. In this study, we report the over-expression, crystallization, and X-ray crystallographic structural determination of TIR-domain from the human TIRAP. Of note, during the course of our experiment, the same TIRAP TIR-domain

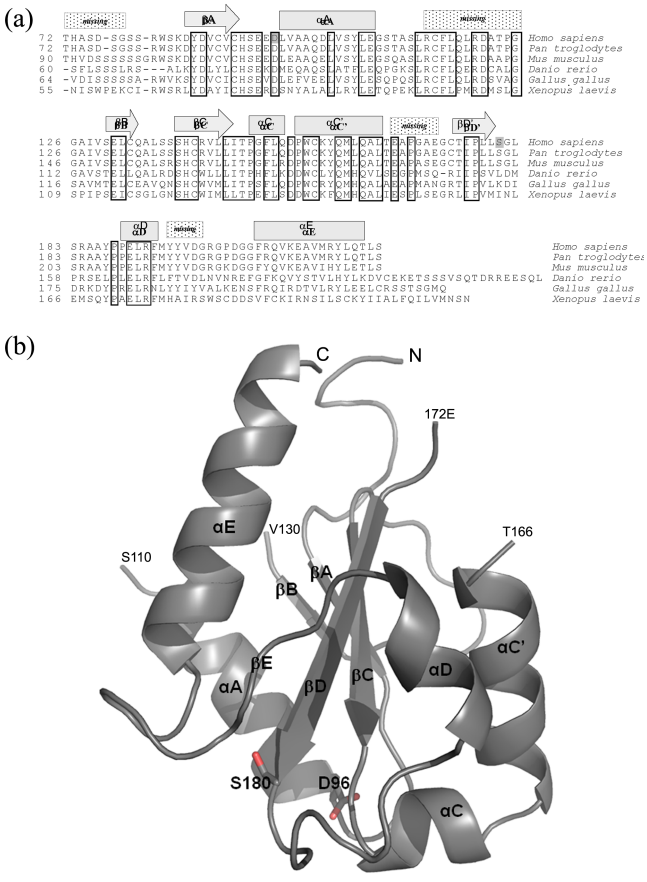

Figure 1. Sequence alignment of TIRAP TIR-domain from selected species (a), and the fold of human TIRAP TIR-domain (b). (a) Amino acid sequence comparison of human, chimpanzee, mouse, zebra fish, chicken and frog TIRAP TIR-domain are shown with secondary structural elements on the top according to the human TIRAP TIR-domain structure. Identical residues are boxed, and human Asp96 and Ser180 residues are highlighted. (b) Schematic ribbon diagram of TIRAP (Mol B) with the five-stranded parallel β-sheet (βA–βE) surrounded by five α-helices (αA, αC, αC', αD and αE) are shown. Residues comprising βE and the loops (αA–βB, 111-129 and αC–βD, 167-171) were not visible in the electron density. Residues of Asp96 and Ser180 whose mutants acquire physiological phenotype are shown as stick models.

structure of 3.0 Å resolution has been determined and reported by another group.[16]

Experimental Methods

The genes encoding the full-length human TIRAP isoform a (residues 1-221) and the TIR-domain (residues 72-221) were PCR-cloned into the vector pET28a (Novagen) using the TIRAP cDNA (ATCC). The proteins were expressed with N-terminal His_6-tag in *E. coli* strain BL21 (DE3) (Stratagene) using kanamycin selection (25 μg/mL). The plasmid-transformed cells were grown at 37 °C in 2 L of LB medium up to OD_{600}=0.6 using a conventional shaker. The recombinant protein expression was induced by 0.5 mM isopropyl β-D-thiogalactopyranoside (IPTG), and the cells were further grown at 25 °C for 16 hrs. Cell pellets were harvested using centrifugation at 4500 g for 10 min at 4 °C, and were re-suspended in an ice-cold lysis buffer (20 mM TRIS at pH 7.5, 500 mM NaCl and 5 mM imidazole). Cell lysates were made from homogenization by sonication, and were centrifuged at 70000 g for 30 min at 4 °C. The supernatants were loaded onto Ni-NTA columns, and washed with a wash buffer (20 mM TRIS at pH 7.5, 500 mM NaCl and 20 mM imidazole). The recombinant proteins were eluted with an elution buffer (20 mM TRIS at pH 7.5, 500 mM NaCl and 200 mM imidazole), and the His_6-tag was removed by adding human thrombin (Roche) to the eluent for 16 hrs at 4 °C. The proteins were further purified using a Superdex 200 (GE Healthcare) sizing column equilibrated with a gel-filtration buffer (50 mM TRIS at pH 7.5, 150 mM NaCl and 2 mM DTT). The protein was further concentrated to ~25 mg/mL by centrifugation using YM-10 Centriprep (Amicon Millipore). Protein concentrations were estimated by absorption at $\lambda = 280$ nm by employing the calculated molar extinction coefficient of 20340 M^{-1} cm^{-1} (SWISS-PROT; http://www.expasy.ch/).

Initial conditions for growing the TIRAP full-length (isoform a, 1-221) crystals were found in commercial screening solutions (Hampton Research). Crystallization screenings were performed at 25 °C by using hanging drop vapour diffusion method in 24-well Linbro plates. Each hanging drop (2 μL) was prepared by mixing equal volumes of the protein solution (~25 mg/mL) and the well solution. Initial single crystals were obtained in a well-solution containing a reservoir of 20% (w/v) PEG 8 K, 0.1 M CAPS at pH 10.5 and 0.2 M NaCl in two months. Mass spectrometry of the crystals detected peptide fragments starting with the TIRAP Asp85, which indicates proteolytic truncations of the full-length TIRAP to only the region that is necessary for the crystal growth (Results not shown). Several clones where designed around Asp85, and tested for protein expression. Only TIRAP 72-221 (TIR-domain) expressed in sufficient amounts required for the protein crystallization. The recombinant protein over-expressed with a final yield of ~50 mg of the purified protein per litre of culture. Crystals of TIRAP TIR-domain appeared within one week from the same condition, but it diffracted to only ~5 Å resolution using the synchrotron radiation. The truncated TIRAP TIR-domain was screened for crystals using the same solutions, and crystals of improved diffraction quality to 3.6 Å resolution appeared in a new condition in two weeks (5% (v/v) PEG 200 and 0.1 M TRIS at pH 8.5). Crystals grew up to approximate dimensions of 5 μm × 20 μm × 300 μm.

For the diffraction experiments, crystal in the growth condition was soaked into the mother liquor containing additional 5% (v/v) glycerol (or ethylene glycol) necessary for cryo-protection prior to exposing them to X-rays from synchrotron radiation under a 100 K nitrogen stream. The diffraction images show isotropic diffraction. A complete set of diffraction data (3.60 Å resolution) were collected at a NSLS beamline (X29) on a CCD detector (ADSC Quantum Q315), and were processed by DENZO and SCALEPACK.[17] The statistics for data collection are summarized in Table 1. The unit cell dimensions are $a = b = 100.3$ Å, $c = 78.9$ Å, and systematic absences and molecular replacement search indicate that the crystal belongs to the tetragonal space group of $P4_322$. A total of 4941 unique reflections had an R_{merge} (on intensity) of 11.8%. Matthews coefficient analysis[18] predicts the crystal with a minimum of two and a maximum of three molecules of TIRAP TIR-domain per asymmetric unit (AU) (Table 1). However, having three molecules per AU is unlikely given the relatively low diffraction power of the crystal at a synchrotron radiation.

Of note, while we were applying the direct phasing methods to solve the human TIRAP TIR-domain structure, Valkov *et al.* have determined the structure to 3.0 Å resolution.[16] The structure was reported with one molecule

Table 1. Data collection and refinement statistics

X-ray wavelength (Å)	1.0809
Temperature (K)	100
Resolution range (Å)	50-3.60
(highest resolution shell)	(3.73-3.60)
Space group	$P4_322$
a, *b*, *c* (Å)	100.25, 100.25, 78.94
Total reflections	376806
Unique reflections	4941 (457)
Redundancy	11.0 (4.7)
Completeness (%)	99.4 (95.6)
Mean $I / \sigma(I)$	19.6 (3.5)
R_{merge} (%)[a]	11.8 (35.5)
Wilson B-factor (Å^2)	85.3
Molecules/AU	2 (3.01, 59.1%)
(Matthews coefficient, % solvent)	3 (2.01, 38.7%)
Refinement R-factor[b] (R_{free}[c])	0.324 (0.346)
RMSD bonds (Å)	0.03516
RMSD angles (°)	3.1518
Average B-factor (main chain) (Å^2)	123.55
Average B-factor (side chain) (Å^2)	112.71

[a] $R_{merge} = \Sigma_h\Sigma_i|I(h,i) - \langle I(h)\rangle|/\Sigma_h \langle I(h)\rangle$, where $I(h,i)$ is the intensity of the ith measurement of reflection h and $\langle I(h)\rangle$ is the mean value of $I(h,i)$ for all i measurements. [b] R-factor = $\Sigma(|F_{obs}|-|F_{calc}|)/\Sigma|F_{obs}|$. [c] R_{free} = R-factor for 10% of randomly selected reflections excluded from the refinement

in the AU. Yet, their crystallization condition, the unit cell parameters, and the diffraction isotropism (10-12% PEG 10,000, 5% PEG 3,350, 0.2 M NaCl, 0.1 M TRIS at pH 7.3 and 20 mM DTT; $a = b = 88.15$ Å, $c = 78.79$ Å, $P4_32_12$; Wilson B-factor = 112.8 Å^2) differs from ours despite the similar TIRAP construct that they have used for the crystallization (human TIR-domain of residues 79-221).

Despite the similar unit cell dimensions of Valkov *et al.*'s and those of our crystal, the proteins pack in a different space group ($P4_32_12$ *vs*. $P4_322$). The locations of the TIRAP molecules from our crystal were determined using the molecular replacement with the Valkov *et al.*'s TIRAP structure as a search model[16] (PDB code 2Y92) in the program PHASER.[19] An automated search routine found two molecules of TIRAP TIR-domain in the crystal AU. The initial model shows reasonable refinement statistics (R_{work} = 0.33/ R_{free} = 0.38, R_{free} = R-factor for 10% of randomly selected reflections excluded from the refinement) which were determined using the program REFMAC5.[20] The model was iteratively modified using Coot[21] and further refined in CNS.[22] The final model contains two TIRAP TIR-domains in the crystal AU (Mol A residues 80-110/127-167/173-194/197-220; Mol B residues 79-110/130-166/172-220) with an R-factor = 0.324/R_{free} = 0.346. Structural figures were rendered with PyMol.[23]

Results and Discussion

The fold of the TIRAP in our crystal is identical to the Valkov *et al.*'s reported structure which composes of a five-stranded parallel β-sheet (βA–βE) surrounded by five α-helices (αA, αC, αC', αD and αE) (Fig. 1(b)). Residues comprising a short αE and the loops (αA–βB and αC–βD) were not visible in our electron density, presumably due to the inherent flexibility. In accordance with Valkov *et al.*'s observation, our structure also displays continuous electron density between residues C89–C134 and C142–C174 which seems to be disulfide bonds. However, we do not discern any DTT-linked cysteines (*i.e.* C91 and C157). Asp96 and Ser180, whose mutants are observed in human polymorphism, are located at one surface of the protein (Fig. 1). The side chain of Asp96 forms a hydrogen bonding network with the side chains of Thr148 (~2.6 Å) and Ser93 (~2.8 Å).

In contrast to Valkov *et al.*'s crystal AU containing one TIRAP molecule, our crystal AU contains two TIRAP molecules related by a two-fold axis (Mol A and Mol B in Fig. 2(a)). Molecular interactions between Mol A and Mol B include a hydrogen bonding interaction between the side chains of Tyr159 (αC') and the main chain carbonyl groups of Pro155 (αC') with ~3.0 Å distance (Fig. 2(a)). Furthermore, Trp156 (αC') and Tyr159 mediate a hydrophobic interaction with ~4.0 Å distance *via* a π-π stacking interaction. The buried solvent accessible surface area between Mol A and Mol B amounted to be ~220 Å^2 when calculated using the PISA server.[24] Since a study[25] using a non-redundant structure database has reported that no known physiological dimer has a contact surface area of less than

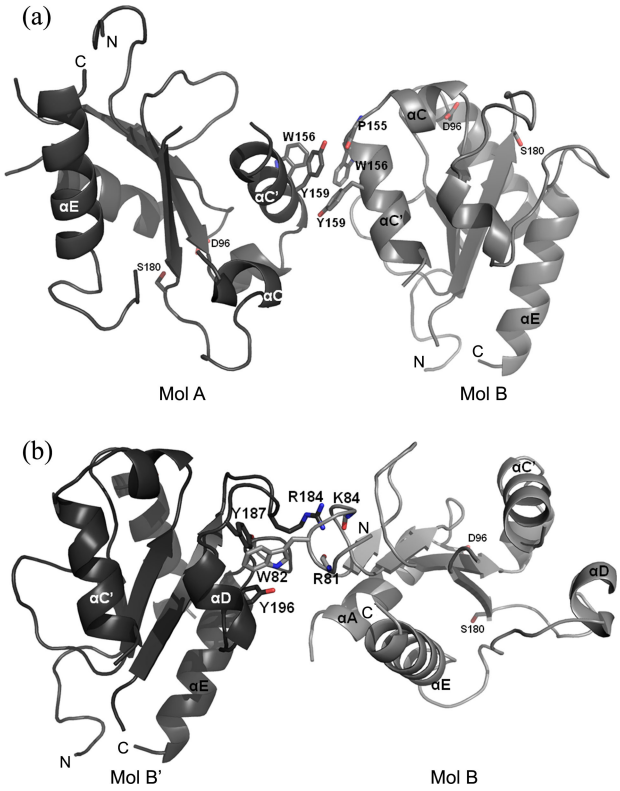

Figure 2. Dimeric interaction of human TIRAP TIR-domain in the crystal asymmetric unit (a) and crystal symmetry generated contact pair of TIRAP TIR-domains (b). (a) TIRAP residues mediating the hydrogen bonding and π-π stacking interaction in the two molecules of the crystal AU (Mol A and Mol B) are shown as stick models. (b) Crystal symmetry interface generated on Mol B (x, y, z) by an symmetry operation (–y, x–1, z–1/4, Mol B') buries ~500 Å^2 accessible surface area. The residues mediating the hydrogen bonding and the hydrophobic pocket are shown as stick models.

500 Å^2, it is difficult to conclude that Mol A/Mol B interface has any physiological significance. This interface may just be a crystal packing artifact.

Although Valkov *et al.* have observed only one TIRAP molecule in their crystal AU, they have reported two potential TIRAP interfaces by analyzing the symmetry pairs within the crystal contact (Interface 1, monomers related by a twofold symmetry axis with ~750 Å^2 buried surface; Interface 2, monomers forming an asymmetric dimer with ~640 Å^2 buried surface). When we similarly analyzed our crystal contacts, an interface with an average of ~490 Å^2 (~470 Å^2 between Mol A symmetry pairs and ~500 Å^2 between Mol B symmetry pairs), which corresponds to Valkov *et al.*'s "Interface 2" was found (Fig. 2(b)). This interface of the crystal contact shown in Figure 2(b) is generated by performing crystal symmetry operation on Mol B (-y, x-1, z-1/4; Mol B'). The discrepancies in our value of the exact buried surface compared to Valkov *et al.*'s "Interface 2" (640 *vs*. 490 Å^2) is due to the missing αA–βB loop from our structure, which mainly mediate the Valkov *et al.*'s "Interface 2". Side chain of Arg184 (of the loop βD–αD in Mol B') which is in hydrogen bonding distance with the

main chain carbonyl oxygen of Arg81 (3.1 Å) and Lys84 (2.6 Å) both near the N-terminal end of Mol B mediates the interface between the two TIRAPs. Also, a hydrophobic pocket is formed *via* the Mol B' side chain residues of Leu179 (loop βD–αD'), Tyr187 (loop βD–αD), Leu191 (helix αD) and Tyr196 (loop αD–βE), and Trp82 (N-terminal end) of Mol B (Fig. 2(b)). Of note, Ser180 and Asp96 are distal from this interface.

Unlike spurious crystal packing interactions, protein interactions with recurring structural themes repeatedly observed between different crystal forms of the same protein have greater likelihood to be biologically relevant.[26] Since the association mode of Mol B/Mol B' interface which also corresponds to the Valkov *et al.*'s "Interface 2" is observed in the two different space groups ($P4_322$ of ours and $P4_32_12$ of Valkov *et al.*'s), we conclude that this interface likely has biological relevance in the TIRAP association inside the cell.

Data Deposition. Atomic coordinates for the human TIRAP TIR-domain and the structure factors for the diffraction data have been deposited in the Protein Data Bank, www.pdb.org (PDB accession code 4FZ5).

Acknowledgments. This work was supported, in whole or in part, by National Institutes of Health Grants R01 DK43123, R01 DK51729 (to S. E. S.), and P30 DK36836 (to Joslin Diabetes Center). Use of the National Synchrotron Light Source, Brookhaven National Laboratory, was supported by the U.S. Department of Energy, Office of Science, Office of Basic Energy Sciences, under Contract No. DE-AC02-98CH10886.

References

1. O'Neill, L. A.; Fitzgerald, K. A.; Bowie, A. G. *Trends Immunol.* **2003**, *24*, 286-290.
2. Yamamoto, M.; Takeda, K.; Akira, S. *Mol. Immunol.* **2004**, *40*, 861-868.
3. Xu, Y.; Tao, X.; Shen, B.; Horng, T.; Medzhitov, R.; Manley, J. L.; Tong, L. *Nature* **2000**, *408*, 111-115.
4. Nyman, T.; Stenmark, P.; Flodin, S.; Johansson, I.; Hammarström, M.; Nordlund, P. *J. Biol. Chem.* **2008**, *283*, 11861-11865.
5. Khan, J. A.; Brint, E. K.; O'Neill, L. A.; Tong, L. *J. Biol. Chem.* **2004**, *279*, 31664-31670.
6. Ohnishi, H.; Tochio, H.; Kato, Z.; Orii, K. E.; Li, A., Kimura, T.; Hiroaki, H.; Kondo, N.; Shirakawa, M. *Proc. Natl. Acad Sci. U S A.* **2009**, *106*, 10260-10265.
7. Chan, S. L.; Low, L. Y.; Hsu, S.; Li, S.; Liu, T.; Santelli, E.; Le Negrate, G.; Reed, J. C.; Woods, V. L., Jr.; Pascual, J. *J. Biol. Chem.* **2009**, *284*, 21386-21392.
8. Chan, S. L.; Mukasa, T.; Santelli, E.; Low, L. Y.; Pascual, J. *Protein Sci.* **2010**, *19*, 155-161.
9. Fitzgerald, K. A.; Palsson-McDermott, E. M.; Bowie, A. G.; Jefferies, C. A.; Mansell, A. S.; Brady, G.; Brint, E.; Dunne, A.; Gray, P.; Harte, M. T.; McMurray, D.; Smith, D. E.; Sims, J. E.; Bird, T. A.; O'Neill, L. A. J. *Nature* **2001**, *413*, 78-83.
10. Horng, T.; Barton, G. M.; Medzhitov, R. *Nature Immun.* **2001**, *2*, 835-841.
11. Horng, T.; Barton, G. M.; Flavell, R. A.; Medzhitov, R. *Nature* **2002**, *420*, 329-333.
12. Kagan, J. C.; Medzhitov, R. *Cell* **2006**, *125*, 943-955.
13. Khor, C. C.; Chapman, S. J.; Vannberg, F. O.; Dunne, A.; Murphy, C.; Ling, E. Y.; Frodsham, A. J.; Walley, A. J.; Kyrieleis, O.; Khan, A.; Aucan, C.; Segal, S. *Nature Genet.* **2007**, *39*, 523-528.
14. Nejentsev, S.; Thye, T.; Szeszko, J. S.; Stevens, H.; Balabanova, Y.; Chinbuah, A. M.; Hibberd, M.; van de Vosse, E.; Alisjahbana, B.; van Crevel, R.; Ottenhoff, T. H. M.; Png, E.; Drobniewski, F.; Todd, J. A.; Seielstad, M.; Horstmann, R. D. *Nature Genet*. **2008**, *40*, 261-262.
15. George, J.; Kubarenko, A. V.; Rautanen, A.; Mills, T. C.; Colak, E.; Kempf, T.; Hill, A. V. S.; Nieters, A.; Weber, A. N. R. *J. Immun.* **2010**, *184*, 3025-3032.
16. Valkov, E.; Stamp, A.; Dimaio, F.; Baker, D.; Verstak, B.; Roversi, P.; Kellie, S.; Sweet, M. J.; Mansell, A.; Gay, N. J.; Martin, J. L.; Kobe, B. *Proc. Natl. Acad Sci. U S A.* **2011**, *108*, 14879-14884.
17. Otwinowski, Z.; Minor, W. *Methods Enzymol.* **1997**, *276*, 307-325.
18. Matthews, B. W. *J. Mol. Biol.* **1968**, *33*, 491-497.
19. McCoy, A. J.; Grosse-Kunstleve, R. W.; Storoni, L. C.; Read, R. J. *Acta Cryst.* **2005**, *D61*, 458-464.
20. Vagin, A. A.; Steiner, R. S.; Lebedev, A. A.; Potterton, L.; McNicholas, S.; Long, F.; Murshudov, G. N. *Acta Cryst.* **2004**, *D60*, 2284-2295.
21. Emsley, P.; Cowtan, K. *Acta Crystallogr. D Biol. Crystallogr.* **2004**, *60*, 2126-2132.
22. Brünger, A. T.; Adams, P. D.; Clore, G. M.; DeLano, W. L.; Gros P.; Grosse-Kunstleve, R. W.; Jiang, J. S.; Kuszewski, J.; Nilges, M.; Pannu, N. S.; Read, R. J.; Rice, L. M.; Simonson, T.; Warren, G. L. *Acta Crystallogr. D Biol. Crystallogr.* **1998**, *54*, 905-921.
23. DeLano, W. L. *The PyMOL Molecular Graphics System*; DeLano Scientific: San Carlos, CA, USA. 2002.
24. Krissinel, E.; Henrick, K. *J. Mol. Biol.* **2007**, *372*, 774-797.
25. Ponstingl, H.; Henrick, K.; Thornton, J. M. *Proteins* **2000**, *41*, 47-57.
26. Shoemaker, B. A.; Panchenko, A. R.; Bryant, S. H. *Protein Sci.* **2006**, *15*, 352-361.